Received: 20 April 2023 | Revised: 2 June 2023 | Accepted: 23 July 2023

DOI: 10.1002/hbm.26443

RESEARCH ARTICLE

WILEY

Association between gene expression and functional-metabolic architecture in Parkinson's disease

Zhenxiang Zang[1,2] | Xiaolong Zhang[3] | Tianbin Song[1,2] | Jiping Li[4] | Binbin Nie[5] | Shanshan Mei[6] | Zhi'an Hu[3] | Yuqing Zhang[4] | Jie Lu[1,2]

[1]Department of Radiology and Nuclear Medicine, Xuanwu Hospital, Capital Medical University, Beijing, China

[2]Beijing Key Laboratory of Magnetic Resonance Imaging and Brain Informatics, Beijing, China

[3]Department of Physiology, College of Basic Medical Sciences, Army Medical University, Chongqing, China

[4]Beijing Institute of Functional Neurosurgery, Xuanwu Hospital, Capital Medical University, Beijing, China

[5]Beijing Engineering Research Center of Radiographic Techniques and Equipment, Institute of High Energy Physics, Chinese Academy of Sciences, Beijing, China

[6]Department of Neurology, Xuanwu Hospital, Capital Medical University, Beijing, China

Correspondence
Jie Lu, Xuanwu Hospital, Changchun Rd No. 45, Beijing 100053, China.
Email: imaginglu@hotmail.com

Funding information
Huizhi Ascent Project of Xuanwu Hospital, Grant/Award Number: HZ2021ZCLJ005

Abstract

Gene expression plays a critical role in the pathogenesis of Parkinson's disease (PD). How gene expression profiles are correlated with functional-metabolic architecture remains obscure. We enrolled 34 PD patients and 25 age-and-sex-matched healthy controls for simultaneous ^{18}F-FDG-PET/functional MRI scanning during resting state. We investigated the functional gradients and the ratio of standard uptake value. Principal component analysis was used to further combine the functional gradients and glucose metabolism into functional-metabolic architecture. Using partial least squares (PLS) regression, we introduced the transcriptomic data from the Allen Institute of Brain Sciences to identify gene expression patterns underlying the affected functional-metabolic architecture in PD. Between-group comparisons revealed significantly higher gradient variation in the visual, somatomotor, dorsal attention, frontoparietal, default mode, and subcortical network ($p_{FDR} < .048$) in PD. Increased FDG-uptake was found in the somatomotor and ventral attention network while decreased FDG-uptake was found in the visual network ($p_{FDR} < .008$). Spatial correlation analysis showed consistently affected patterns of functional gradients and metabolism ($p = 2.47 \times 10^{-8}$). PLS analysis and gene ontological analyses further revealed that genes were mainly enriched for metabolic, catabolic, cellular response to ions, and regulation of DNA transcription and RNA biosynthesis. In conclusion, our study provided genetic pathological mechanism to explain imaging-defined brain functional-metabolic architecture of PD.

KEYWORDS
gene expression, glucose metabolism, gradients, hybrid PET/MRI, Parkinson's disease

1 | INTRODUCTION

Genetic influence is one of the most crucial and fundamental risk factors for revealing the pathogenesis and pathological mechanism of PD (Nalls et al., 2019; Scherzer et al., 2007; Simunovic et al., 2008). For example, mutations in LRRK2 are closely associated with the form of PD (Klein & Westenberger, 2012). On the macro system-level, recent

Abbreviations: DMN, default mode network; DAN, dorsal attention network; FD, frame-wise displacement; FPN, frontoparietal network; GO, gene ontology; HCs, healthy controls; LN, limbic network; PD, Parkinson's disease; PLS, partial least square; PC, principle component; SUVr, ratio of standard uptake value; SMN, somatomotor network; SN, subcortical network; VAN, ventral attention network; VN, visual network.

Zhenxiang Zang and Xiaolong Zhang contributed equally to this study.

neuroimaging studies have begun to shed light on mapping gene expression profiles onto structural networks in PD, and provided promising insights that immune-related (Freeze et al., 2019), and mRNA as well as chromosome metabolic-related (Zarkali et al., 2020) genetic pathways may initiate the disease process via impairment of structural connectome. Functional MRI (fMRI) and ^{18}F-FDG-PET studies also showed massive functional as well as metabolic impairments of not only the basal ganglia motor loop, but also non-motor networks in PD patients (Ma et al., 2007; P. Wu et al., 2013; T. Wu et al., 2011). However, how gene expression profiles are associated with the functional-metabolic architecture in PD remains poorly understood. Studying the genetic influence on the functional-metabolic architecture could not only deepen the understanding of PD pathology, but also benefit potential therapeutic intervention of this devastating neurodegeneration disease.

Neurodegeneration of the dopaminergic neurons and accumulation of Lewy bodies in the substantia nigra is the pathological hallmark (DeLong, 1990; McGregor & Nelson, 2019), which may further disrupt basal ganglia loops (Ji et al., 2018; Ko et al., 2018; Ruppert et al., 2020). In addition, recent studies have acknowledged alterations of widespread functional architectures in the visual network (VN; Weil et al., 2016), the frontoparietal network (FPN; Cascone et al., 2021; Vervoort et al., 2016), and the default mode network (DMN; Ruppert et al., 2021) in PD patients, demonstrating impairments of multifunctional principles. The human cerebral cortex is an integration of multiple functional principles that process different basic categories of information (VN, SMN, etc.) (Damoiseaux et al., 2006; Power et al., 2011). This characteristic of the brain network has been recently well-validated by the diffusion embedding approach (Coifman et al., 2005) that projects both local and long-distance connections into a common space for representation of gradual transitions among distinct functional epicenters (Margulies et al., 2016). Since then, the diffusion embedding approach has been successfully applied to characterize abnormal transactions of functional connectivity gradients in epilepsy (Caciagli et al., 2022), autism (Hong et al., 2019), and major depression disorder (Xia, Liu, et al., 2022). Investigation of the functional gradients disruption in PD patients is critical for describing the pathological profiles from the perspective of macro system-level.

For PD patients, ^{18}F-FDG-PET studies have revealed a high coincidence between the spatial patterns of the abnormal glucose metabolism and the disrupted functional networks, including increased FDG-uptake in the cortical–basal ganglia–thalamus–cortical loop and reduction of FDG-uptake in the visual area and the frontal–parietal networks (Albrecht et al., 2019; Ruppert et al., 2020; Schindlbeck & Eidelberg, 2018). In addition, glucose metabolism is the basis of functional network as most of the energy consumption is dedicated to neural communication (Hyder et al., 2013). Therefore, glucose metabolism plays both physiologically and pathologically a critical role in the system-level architecture of PD patients. Combination of functional gradients and glucose metabolism could benefit thorough examinations of the association between gene expression profiles and the brain functional-metabolic architecture.

Here, we applied hybrid PET/MRI scanning to simultaneously measure the network functional gradients and glucose metabolism. We first asked how the network functional gradients and glucose metabolism are impaired in PD. By introducing transcriptomic gene expression data from the Allen Brain Atlas (http://www.brain-map.org), we further intended to investigate the neural biological process underlying brain functional-metabolic architecture in PD.

2 | METHODS

2.1 | Participants

The current study was approved by the ethic committee of Xuanwu Hospital. All participants provided written informed consent. The hybrid PET/MRI dataset was published in our previous studies (Zang, Song, Li, Nie, et al., 2022; Zang, Song, Li, Yan, et al., 2022). All PD patients were diagnosed with the movement disorder-PD criteria (Postuma et al., 2015; Postuma et al., 2018). We excluded subjects with over 30% time points that exceeded 0.5 mm frame-wise displacement (FD) during RS-fMRI scan (Yan et al., 2013). Then, 8 out of 42 PD patients were excluded due to excessive FD, leaving 34 PD patients and 25 age- and sex-matched healthy controls (HCs) for further analyses. This exclusion criterion was used to ensure that the PD patients would not show significantly large head motion than that of the HCs. All participants were right-handed, and reported no history of head trauma, cerebral vascular disease, or psychiatric disease. The HCs reported no history of drug abuse, neurological and psychiatric conditions. PD patients were instructed to not use dopaminergic medication for at least 12 h prior to the scan. Detailed information on all our subjects is provided in Table 1.

2.2 | Data acquisition

All data were acquired on a hybrid PET/MRI scanner (uPMR790, UIH, Shanghai, China). All patients were fasted for at least 6 h before PET/MR examination. The injected dose of ^{18}F-FDG was 3.7 MBq/kg. The detailed acquisition parameters of resting-state fMRI and ^{18}F-FDG data are provided in the supplementary information.

2.3 | fMRI data preprocessing

Image preprocessing was performed using the standard routine in SPM12 (https://www.fil.ion.ucl.ac.uk/spm/software/spm12/). The image preprocessing routine included head motion correction, slice timing, normalization of functional images via T1 images (resampled to $3 \times 3 \times 3$ mm^3), and spatial smoothing with an 8-mm full width at half maximum (FWHM) Gaussian kernel. After spatial smoothing, we further regressed out the time series of white matter (99% probability SPM map), cerebrospinal fluid (90% probability SPM map) (Zang et al., 2018), global mean time course, six head motion parameters

TABLE 1 Demographic characteristics of subjects.

	HC	PD	Test statistics	*p*-Value
Number	25	34		
Sex (female:male)	17:8	21:13	$\chi^2 = 0.24$	.62
Age (mean [SD])	60.00 (4.54)	62.32 (6.40)	$T = -1.55$	.13
FD (mean [SD])	0.22 (0.09)	0.21 (0.08)	$T = 0.53$	.60
HY-stage (mean [SD])		3.00 (0.83)		
UPDRS III (mean [SD])		59.71 (15.00)		
Disease duration (mean [SD])		9.59 (4.04)		
Dopaminergic daily dose (mg/day, mean [SD])		879.88 (432.81)		
MMSE (mean [SD])		23.07 (3.66)		
MoCA (mean [SD])		26.67 (2.97)		

Abbreviations: FD, frame-wise displacement; HC, healthy control; HY-stage, Hoehn–Yahr stage; MMSE, Mini-Mental State Examination; MoCA, Montreal Cognitive Assessment; PD, Parkinson's disease; SD, standard deviation; UPDRS III, Unified Parkinson's Disease Rating Scale III.

from the realignment step, and the FD (Power et al., 2012). We then applied band-pass filtering of 0.01–0.1 Hz and head motion scrubbing (Power et al., 2014). The head motion scrubbing was applied to further reduce the dynamic head motion influence on the brain time series.

2.4 | PET data processing

PET images were first preprocessed in SPM12 for spatial normalization via T1 images. An 8-mm FWHM Gaussian kernel was used for spatial smoothing.

A data-driven approach was applied for the identification of reference region during ratio of standard uptake value (SUVr) calculation (Nie et al., 2018). First, whole brain was defined as the reference region, named Ref0. Second, Ref0 was chosen for global confounds in a voxel-wised two-sample *t* test between the preprocessed images of PD patients and HC. Third, the significant region was defined with a threshold of $p < .05$ (uncorrected), named SigRegion. Then, we excluded SigRegion from Ref0 to define the new reference region, named Ref1. Next, we replaced Ref0 with Ref1 and repeated the steps 2–5 until the residual deviation between the Ref1 and Ref0 was reduced by less than 5%. The newest Ref1 was accepted as the data-driven unbiased reference region for SUVr calculation.

One patient was excluded due to large imaging artifacts, resulting in 58 subjects in total for further PET-related analyses (25 HC, 33 PD).

2.5 | Construction of functional network gradients

The original description of functional gradients was at the vertex-wise level, which implies decomposing a connectivity matrix with a dimension of tens of thousands (Margulies et al., 2016). To gain relatively high spatial resolution while reducing the computational burden, the cerebrum was parcellated into 3568 brain areas upon the compact parcellation approach (Zalesky et al., 2010). The largest parcellated areas (540 mm^3) were no larger than twice the smallest areas (270 mm^3). Averaged time series were extracted from the parcellated brain areas. Individual functional connectivity matrix was constructed using Fisher's Z-transformed Pearson's correlation coefficient. A group-averaged functional connectivity matrix was also obtained via the mean Z-transformed correlation coefficient of both HCs and PD.

Next, in line with previous studies (Dong et al., 2021; Hong et al., 2019; Margulies et al., 2016; Xia, Liu, et al., 2022), both the individual and group-averaged functional connectivity matrices were thresholded with retaining the values of the top 10% of connections per row and converted into normalized angle matrices using cosine similarity (Xia, Liu, et al., 2022). Then, we used the diffusion embedding approach to decompose the individual and group-averaged matrices into multiple gradients denoting the connectivity pattern variance in the functional connectivity matrix using BrainSpace (Vos de Wael et al., 2020). The gradient score of each brain region reflects the position of the brain region along the corresponding gradient axis which is determined by the difference in the connectivity patterns. Individual gradients were further aligned to the group-template gradients using Procrustes analysis (Hong et al., 2019). Considering the straightforward interpretability of the first two gradients (Margulies et al., 2016), we focused on the first two gradients as did in previous studies (Hong et al., 2019; Xia, Xia, et al., 2022). To depict the dispersion of the principal gradients along the two axes, we calculated the standard deviations (SDs) of the first two gradients within Yeo's seven well-established cortical networks (VN, SMN, dorsal attention network [DAN], ventral attention network [VAN], limbic network [LN], FPN, DMN) (Yeo et al., 2011) and the subcortical network (SN). The SN consisted of the putamen, caudate, globus pallidus, and thalamus from the automated anatomical labeling template (Tzourio-Mazoyer et al., 2002).

2.6 | Group comparisons of functional gradients and FDG-uptake

We compared the explanation ratios and the dispersions of the first two gradients between HC and PD using a general linear model (GLM) with the Statistical Package for the Social Sciences 24 (SPSS24,

https://www.ibm.com/analytics/spss-statistics-software) while correcting for age, sex and FD to further remove the effects of age, sex, and FD on between-group comparisons. For FDG-uptake analysis, we averaged the values of voxels within each Yeo's network as well as the SN and compared them between groups using a GLM while correcting for age and sex. And we corrected for multiple comparisons using false discovery rate (FDR; $Q < 0.05$).

2.7 | Associations between cortical functional-metabolic architecture and gene expression

We then followed the methods of Thomas et al. (2021) to examine the association between impairments of functional-metabolic architecture in PD and the healthy brain transcriptome. Considering the marked transcriptional differences between cortical and subcortical regions and that the transcriptomic data were available from six donors for the left hemisphere (Hawrylycz et al., 2015; Thomas et al., 2021), we only conducted gene expression analysis within the left cortical regions. Each tissue sample was assigned to one of Glasser regions using its coordinates. Genes with expression levels above a background threshold of 50% were selected and gene expression data were normalized across the left hemisphere. We mapped the 3568 parcellated brain areas into Glasser's atlas (Glasser et al., 2016) and averaged the gradients and FDG-uptake accordingly. For each region of interest (ROI) of the Glasser atlas, we normalized PD's functional gradients score and FDG-uptake to the HCs using a z-score transformation:

$$Z_{ROI} = \frac{ROI_{PD} - \text{mean}(ROI_{HCs})}{\text{std}(ROI_{HCs})}$$

where Z_{ROI} represents the normalized PD's functional gradients score and FDG-uptake, ROI_{PD} and ROI_{HCs} are the raw functional gradients score and FDG-uptake of each Glasser's ROI. Finally, 180 Z_{ROI} were generated across the left cortical areas.

Statistically significant differences between the ROIs were probed using t tests and are reported at $p < .05$. To combine the PD-related alternations in the two neuroimaging measures together, we performed a group-level principal component analysis (PCA) on the normalized ROI means of principal gradients and FDG-uptake using SPSS24.The first component was defined as the functional-metabolic architecture of PD.

The preprocessed gene expression matrix (180 cortical regions × 15,745 genes) was obtained at (https://github.com/gecthomas/QSM_and_AHBA_transcription_in_PD; last updated March 26, 2021) (Thomas et al., 2021). Then, we utilized partial least squares (PLS) regression to examine the associations between healthy brain transcriptome (X) and cortical functional-metabolic architecture of PD (Y). We performed 10,000 permutations based on sphere-projection-rotations (Váša et al., 2018) of the cortical functional-metabolic architecture to test the null hypothesis that components explained no more variation than chance. The first PLS component (PLS1) from X that significantly explained more variation than chance and showed the maximum covariance with Y was used to weigh and rank genes-the predictor variables. Bootstrapping was performed to estimate the variability of each gene's weight on PLS1 and the ratio of each gene's weight to the bootstrapped standard error was used to rank its contribution to the PLS1. We used Bonferroni correction to test the null hypothesis of zero weight for each gene to take the winner's curse bias into account (Bigdeli et al., 2016). And only genes that survived this correction ($p_{Bonferroni} < .05$) were included in the enrichment analysis.

2.8 | Gene ontological and validation analyses

We utilized the g:Profiler package (Raudvere et al., 2019) to perform the gene ontological (GO) enrichment analysis for the significantly weighted genes identified by PLS components. Upweighted and downweighted genes were analyzed separately. We only included GO terms that were significantly enriched at $p < .05$ after correcting for multiple comparisons using the g:SCS package (Raudvere et al., 2019). GO terms that contain more than 2500 genes were also excluded because they are too general. Additionally, we performed GO enrichment analysis for a random and spatial-spin permutation of the cortical functional-metabolic architecture and compared the GO terms to those from the main analysis. The detailed spatial-spin permutation method is provided in SI.

Since the PLS regression analysis was only performed within the cortical areas, we validated the main results by estimating the principal gradients excluding the subcortical area and replicating the PLS regression and GO analyses. Figure 1 displays a flowchart of data processing. Cortical mapping shown in Figure 1 was performed using BrainNet Viewer (Xia et al., 2013).

2.9 | Contribution of each network in the regression analysis

Finally, in order to examine how each network influences the estimation of the association between functional-metabolic architecture and gene expression profiles, we applied a leave-one-network-out approach. In detail, we excluded one network from the PLS regression each time and then assessed the influence of this network on the regression analysis. We focus on the number of newly changed genes, the number of overlapped genes as well as the similarity of GO terms.

2.10 | Comparison with external PD postmortem-derived gene expression information

To test whether genes differentially expressed in PD can help to explain the gene expression patterns of PLS1 here, we matched the genes identified in cortical regions in PD to the genes defined by PLS1. Genes that were differentially expressed in PD and later disease stage relative to controls were provided by Thomas et al. (2021). We then investigated whether genes provided by Thomas were

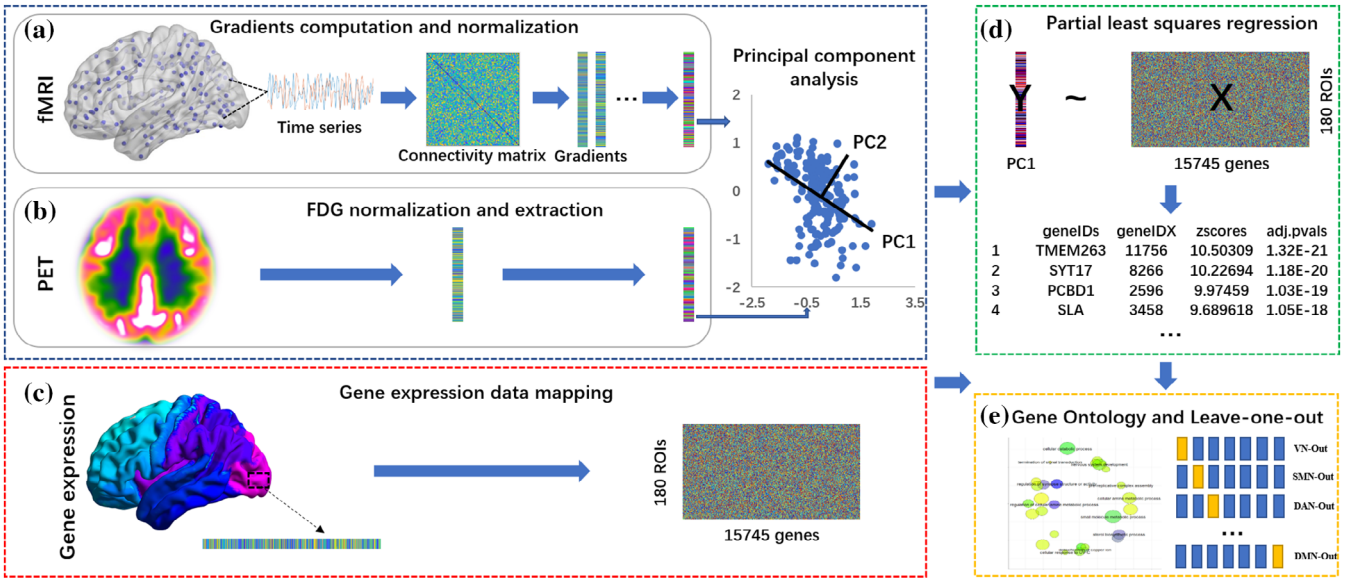

FIGURE 1 Methodology framework. Panel (a): Principal gradients were computed based on functional connectome, averaged within 180 cortical regions and then normalized using a z-score transformation. Panel (b): FDG-uptake was extracted within 180 cortical regions and also normalized using a z-score transformation. The alternations in gradients and FDG-uptake were combined using a principal component analysis. Panel (c): Samples of gene expression data were mapped to 180 cortical regions and were used to create the averaged expression matrix of 15,745 genes in those regions. Panel (d): A partial least squares regression was used to explore the association of gene expression (X) and cortical functional-metabolic alternations in Parkinson's disease (Y). The component that explained the maximum variance was used to rank the contributions of genes to the component. Panel (e): Genes that were significant after correction underwent gene ontological analyses for biological processes. In addition, the leave-one-out validation approach was carried out to evaluate the influence of each network on the relationship between gene expression profiles and functional-metabolic architecture.

significantly more positively or negatively weighted than chance by using 10,000 random permutations of the same sample size.

2.11 | Relationships between clinical measures and functional-metabolic architecture

The group-level PCA allowed us to examine the spatial profiles of the functional-metabolic architecture and the association with gene expression, yet was difficult for investigation of clinical relevance on an individual level. To further explore the relationship between functional-metabolic architecture of PD and clinical measures including Unified Parkinson's Disease Rating Scale III (UPDRS III score), Hoehn–Yahr stage (H–Y stage), disease duration, Mini-Mental State Examination (MMSE), and Montreal Cognitive Assessment (MoCA). We in addition performed an individual-level PCA on functional gradients and FDG-uptake for each network separately and then computed the partial Pearson's correlation coefficients between the resultant component and clinical measures in PD group using age and sex as covariates.

3 | RESULTS

3.1 | Demographic data

We did not find any significant differences in age ($p = .13$), FD ($p = .60$), or sex ($p = .62$) between HC and PD. Then, 34 PD patients and 25 HCs were used for fMRI analysis and 58 subjects (33 PD and 25 HCs, PET image from one PD were excluded due to huge image noise) were analyzed for PET. Joint analyses of PET/fMRI were carried out based on 58 subjects (33 PD and 25 HCs). Details about the demographic characteristics can be found at Table 1.

3.2 | Principal gradients comparisons

By applying diffusion embedding approach to a group-averaged functional connectome, we obtained a group template of principal gradients. The first gradient explained 10.80% of the variance and distributed from VN to the SMN, while the second gradient explained 10.38% of the variance and ran from primary VN/SMN to the DMN (Figure 2a).

We did not find any group difference in the explanation ratio of the first ($F(1, 55) = 0.007$, $p = .934$) and second gradient ($F(1, 55) = 0.399$, $p = .53$), implying that the following between-group comparisons of principal gradients would not be affected by explanation ratios.

We first investigated whether the network dispersion defined by the first two gradients together showed any group difference. Since we did not find any significant difference in the network dispersion of gradient 1 and 2 combined across eight networks, we next compared the SD of the first two gradients separately. For the first gradient, we found significantly higher variation in VN ($F(1, 54) = 10.012$, $p_{FDR} = .048$, $\eta^2 = 0.156$); SMN ($F(1, 54) = 8.138$, $p_{FDR} = .027$,

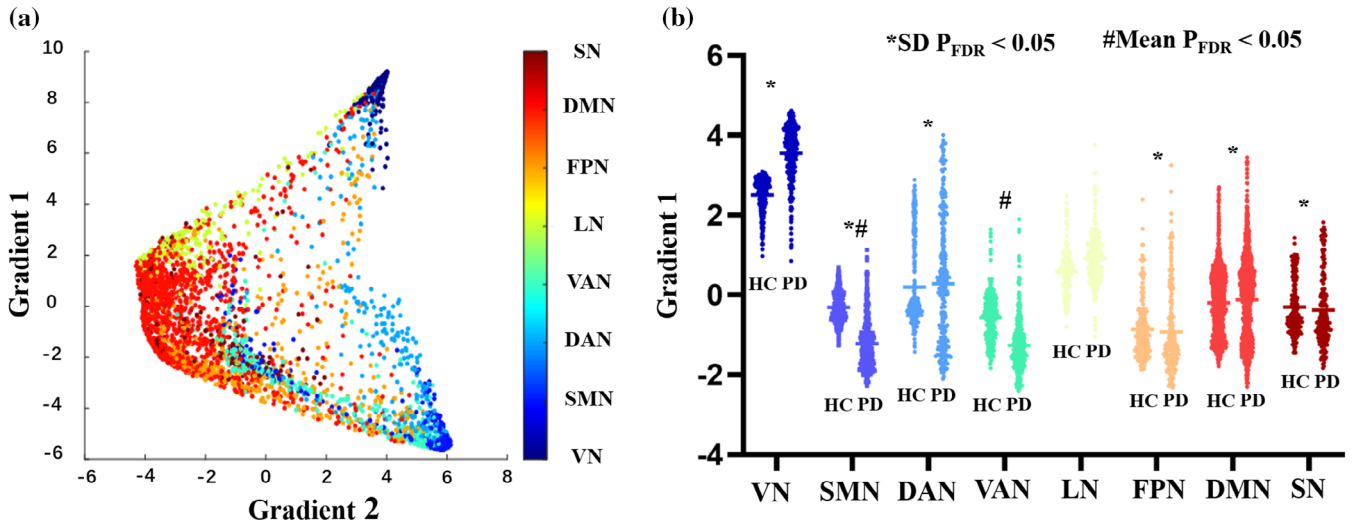

FIGURE 2 Group differences of the first gradient across networks between healthy controls (HCs) and patients with Parkinson's disease (PD). Panel a: The scatterplot of the first two gradients from group template. Panel b: Distribution of the first group-averaged gradient across eight networks. Star (*) denotes significant difference in the standard deviation (SD) of the first gradient between PD and HC after correcting for multiple comparisons. Hash (#) denotes significant differences in the mean of line denotes the mean of the first gradient between PD and HC after correcting for multiple comparisons. DAN, dorsal attention network; DMN, default mode network; FPN, frontoparietal network; LN, limbic network; SMN, somatomotor network; SN, subcortical network; VAN, ventral attention network; VN, visual network.

$\eta^2 = 0.131$); DAN ($F(1, 54) = 7.377$, $p_{FDR} = .032$, $\eta^2 = 0.120$); FPN ($F(1, 54) = 7.512$, $p_{FDR} = .029$, $\eta^2 = 0.122$); DMN ($F(1, 54) = 9.166$, $p_{FDR} = .032$, $\eta^2 = 0.145$); and SN ($F(1, 54) = 6.972$, $p_{FDR} = .029$, $\eta^2 = 0.114$) of PD after correcting for multiple comparisons (Figure 2b). Except for differences of SD of the first gradient, we also found significantly lower mean gradients of SMN ($F(1, 54) = 14.521$, $p_{FDR} = .0014$, $\eta^2 = 0.212$) and VAN ($F(1, 54) = 17.361$, $p_{FDR} = 9.6 \times 10^{-4}$ $\eta^2 = 0.243$) in PD. We did not find any significant group difference for the second gradient. Age, sex, and FD were controlled as covariates of noninterests.

3.3 | FDG-uptake comparisons

After averaging the FDG-uptake within each network, we found significantly lower FDG values in VN ($F(1, 54) = 23.40$, $p_{FDR} = 4.4 \times 10^{-5}$, $\eta^2 = 0.302$, Supplementary Figure 1a), and higher FDG values in SMN ($F(1, 54) = 26.45$, $p_{FDR} = 3.2 \times 10^{-5}$, $\eta^2 = 0.329$, Supplementary Figure 1b) and VAN ($F(1, 54) = 9.75$ $p_{FDR} = .008$, $\eta^2 = 0.153$, Supplementary Figure 1c) in PD than HC after correcting for multiple comparisons. Age and sex were controlled as covariates of noninterests.

3.4 | Relationship between clinical measures and functional-metabolic architecture

To construct individual functional-metabolic architecture, we performed an individual-level PCA on the mean gradients and FDG-uptake within each network. Since only the mean gradients of SMN showed significant correlation with its FDG-uptake ($r = -.301$, $p = .021$), we only tested the partial correlation of functional-metabolic architecture of SMN and clinical measures. The first component explained 65.07% of variance and was defined as the functional-metabolic architecture of SMN: higher component score corresponds to lower FDG-uptake and higher mean gradients. We found significantly negative association between functional-metabolic architecture of SMN and UPDRS III ($r = -.421$, $p = .018$, Supplementary Figure 2) across all patients, while HY-stage ($r = -.288$, $p = .116$), disease duration ($r = .127$, $p = .497$), MMSE ($r = .142$, $p = .453$), and MoCA ($r = .234$, $p = .271$) did not show significant association did not show significant association.

3.5 | Association between gene expression and functional-metabolic architecture

To investigate the genetic mechanisms underlying the alternations both functional gradients and glucose metabolism in PD, we combined the effects of two neuroimaging measures in the cortical regions of the left hemisphere. This was because the gene expression data of the let hemisphere was available for six donors compared to two with right hemisphere. There was a significant correlation between the normalized gradients and FDG-uptake ($r = -.40$, $p = 2.47 \times 10^{-8}$, Figure 3) across brain regions. Therefore, we performed a group-level PCA on the functional gradients and FDG-uptake of PD's cortical regions normalized to the control mean.

The first principal component of the combined functional gradients and glucose metabolism (PC1, Figure 4a) explained 70.3% of the variance and was positively correlated with normalized FDG-uptake

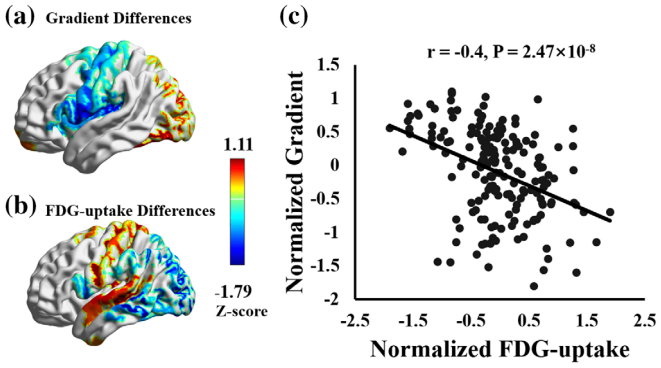

FIGURE 3 Spatial correlation of normalized gradients and FDG-uptake. Parkinson's disease (PD's) region of interest (ROI) means were normalized to controls' mean using a z-score transformation. (a) Normalized gradients and (b) FDG-uptake of cortical regions that showed significant group differences after correcting for multiple comparisons. (c) Significant spatial correlation of normalized gradients and FDG-uptake. Each dot represents one of the 180 cortical regions.

($r = .878$) and negatively correlated with the normalized first gradients ($r = -.791$): higher component score corresponds to higher FDG-uptake and lower gradients in PD compared to HCs. We used PC1 to represent the cortical functional-metabolic architecture in PD for gene expression analyses.

Then, we used PLS regression to examine the association between healthy brain gene expression and cortical functional-metabolic architecture of PD. While taking all seven cortical networks into account, the first component explaining the most variance (27.8%) did not significantly explain more variance than chance ($p = .0879$). We excluded LN in the following PLS regression, because there was no significant difference in either principal gradients or FDG-uptake of LN between PD and HC.

PLS regression on the six cortical networks revealed that the first (PLS1) and third (PLS3) components together explained 48.99% of the variance in the PD-related alternations in functional-metabolic architecture, which were significantly higher than chance. In detail, the PLS1 explained the most (32.38%) variance of the functional-metabolic architecture ($p_{FDR} = .0271$, permutation tests, Figure 4b) and was positively correlated with the functional-metabolic architecture ($r = .569$, $p = 1.25 \times 10^{-15}$, permutation tests, Figure 4c), meaning that genes that were positively correlated with PLS1 were also more highly expressed in cortical brain regions with higher functional-metabolic architecture (higher FDG-uptake and lower gradients). And PLS3 explained the second most (16.61%) variance of the functional-metabolic architecture ($p_{FDR} = .0261$, permutation tests, Supplementary Figure 3a) and was also positively correlated with the functional-metabolic architecture ($r = .408$, $p = 5.03 \times 10^{-8}$, permutation tests, Supplementary Figure 3b). PLS1 represented transcriptional profiles with high expression in VAN and DMN but low expression in VN (Supplementary Figure 4a), while PLS3 represented transcriptional profiles with high expression in SMN and VAN but low expression in DAN (Supplementary Figure 4b). By using PLS1 to rank and select significantly weighted genes, we obtained 920 upweighted genes and 527 downweighted genes and assessed these lists separately. And by using PLS3 to rank and select significantly weighted genes, we obtained 169 upweighted genes and 120 downweighted genes.

Based on cortical connectivity matrix, we calculated again the principal gradients and replicated the PLS regression and ontological analyses. Our main results were remained: alternations in principal gradients and FDG-uptake were spatially correlated; PLS1 and PLS3 identified similar gene lists (SI, Supplementary Figure 5).

3.6 | Gene ontological analysis

Using GO analyses, we found a set of biological pathways enriched in upweighted and downweighted genes. For PLS1, upweighted genes were mainly enriched for GO terms relating to copper ion detoxification and stress response, cellular and molecular metabolic process, catabolic process, biosynthetic process and regulation of synapse activity (Figure 5a). Downweighted genes were mainly enriched for GO terms relating to neuron and nervous system development, RNA metabolic and biosynthetic process and transcriptional regulation (Figure 5b). The top 15 pathways of the PLS1 are listed in Table 2. While for PLS3, genes more were mainly enriched for GO terms relating to jasmonic acid, basal ganglia development and ion transport (Supplementary Table 1 and 2). Go terms shown in all figures were plotted using REVIGO (Supek et al., 2011).

We performed two control analyses: spatial-spin permutation of the cortical data; random permutation of the cortical data. For spatial-spin permutation, upweighted genes were mainly enriched for transmembrane transport (Supplementary Table 3), and downweighted genes were not enriched for any biological pathways. For random permutation, upweighted genes were not enriched for any biological pathways and downweighted genes were enriched for repair and methylation (Supplementary Table 4).

3.7 | Specific contributions of six networks onto GO analyses

Next, we compared the relative contribution of each network to identify the underlying associations of gene expression and cortical functional-metabolic architecture by leaving out one network each time in the PLS regression. Then, we compared the resultant gene lists and GO terms to those based on six networks. While leaving out VN, the number of significantly weighted genes ranked by PLS1 ($p = .0021$, permutation tests) decreased greatest (upweighted: 356, downweighted: 166). For SMN, the number of significantly weighted genes ranked by PLS1 ($p = .0016$, permutation tests) increased greatest (upweighted: 1897, downweighted: 1445), and they included most of the genes identified by six networks (upweighted: 916 of 920, downweighted: 526 of 527). While for other four networks (DAN, VAN, FPN, DMN), the number of significantly weighted genes ranked by PLS1 did not change much and most of these genes existed in the gene lists identified by six networks

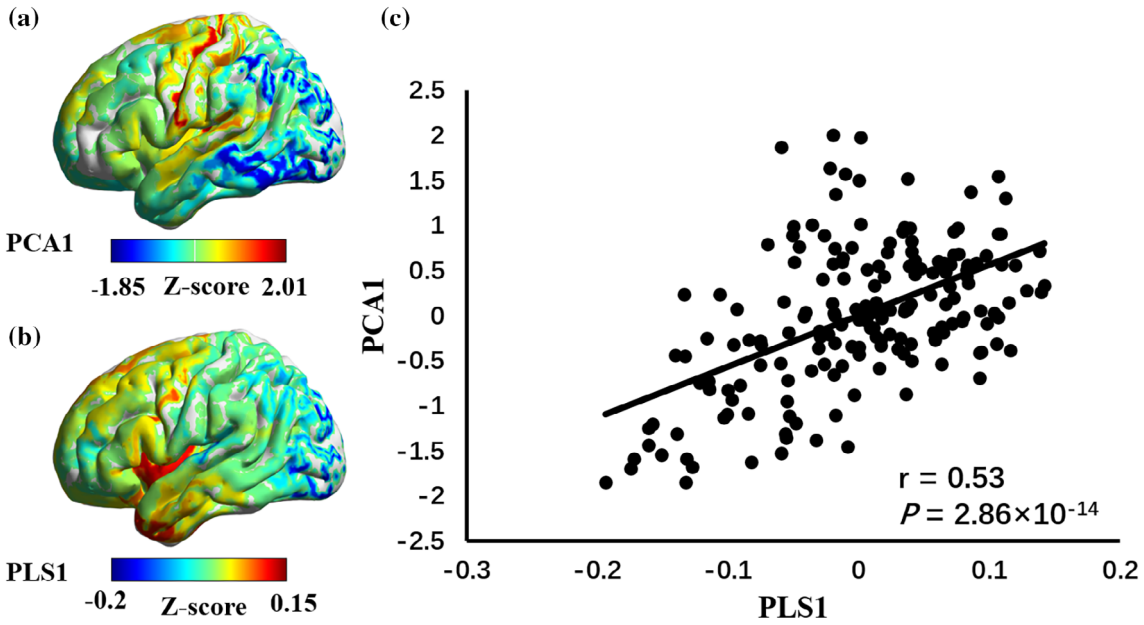

FIGURE 4 Spatial correlation of the weights of regional partial least squares (PLS) components and cortical functional-metabolic alternations in Parkinson's disease (PD). Panel (a) shows the cortical map of the functional-metabolic architecture on the alternations in principal gradients and FDG-uptake in PD. Panel (b) shows similar spatial pattern to the regional weighted sum of gene expression scores defined by the first (PLS1) PLS components. The spatial distribution of functional-metabolic architecture was significantly correlated with the PLS1 (Panel c).

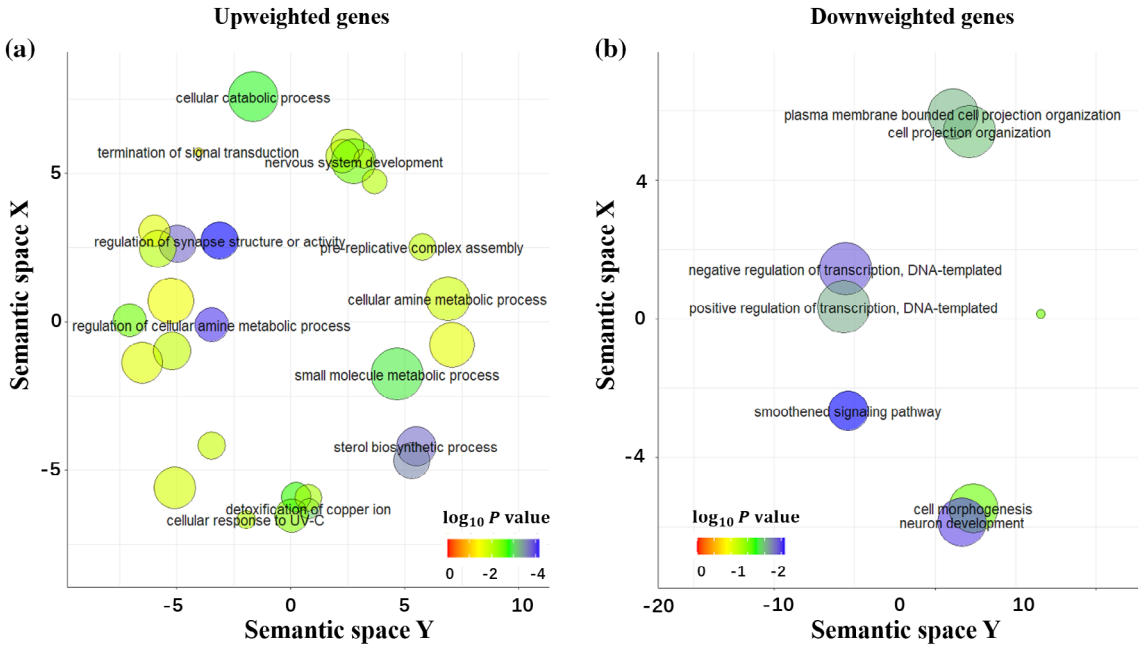

FIGURE 5 The gene ontological terms for biological pathways in enrichment analysis. The gene ontological terms for biological pathways enriching in significantly upweighted (Panel a) and downweighted (Panel b) genes defined by partial least squares (PLS) component 1. The terms are plotted in sematic space with more similar terms located closer. Significant terms at g:SCS corrected $p < .05$ are showed and larger, colder circles represent greater significance.

(Figure 6, Supplementary Table 5). We did not find significant correlation between the number of ROIs and the changes in number of significantly weighted genes ($p = .616$), implying no effect of the number of ROIs in each network on the results. Furthermore, removing VN, SMN, and DAN in the PLS regression greatly changed the significantly enriched GO biological processes (see Supplementary Table 6–11). Venn diagrams shown in Figure 6 were plotted using BioVenn (Hulsen et al., 2008).

TABLE 2 Top 15 GO terms for biological pathways enriching genes defined by PLS1.

GO terms of upweighted genes				GO terms of downweighted genes			
Term ID	**Term name**	***p*-Value**	**Size**	**Term ID**	**Term name**	***p*-Value**	**Size**
GO:0050803	Regulation of synapse structure or activity	7.24×10^{-5}	212	GO:0007224	Smoothened signaling pathway	.0035	142
GO:0033238	Regulation of cellular amine metabolic process	1.01×10^{-4}	55	GO:0048666	Neuron development	.0047	1108
GO:0050807	Regulation of synapse organization	1.90×10^{-4}	206	GO:0045892	Negative regulation of transcription, DNA-templated	.0055	1293
GO:0016126	Sterol biosynthetic process	2.04×10^{-4}	60	GO:1903507	Negative regulation of nucleic acid-templated transcription	.0058	1295
GO:1902653	Secondary alcohol biosynthetic process	3.11×10^{-4}	53	GO:1902679	Negative regulation of RNA biosynthetic process	.006	1297
GO:0006695	Cholesterol biosynthetic process	3.11×10^{-4}	53	GO:0051253	Negative regulation of RNA metabolic process	.0092	1409
GO:0010273	Detoxification of copper ion	8.86×10^{-4}	14	GO:0007399	Nervous system development	.0104	2430
GO:1990169	Stress response to copper ion	8.86×10^{-4}	14	GO:1903508	Positive regulation of nucleic acid-templated transcription	.0113	1636
GO:0044281	Small molecule metabolic process	1.31×10^{-3}	1796	GO:0045893	Positive regulation of transcription, DNA-templated	.0113	1636
GO:1905606	Regulation of presynapse assembly	1.48×10^{-3}	34	GO:0120036	Plasma membrane bounded cell projection organization	.0121	1485
GO:0099174	Regulation of presynapse organization	1.48×10^{-3}	34	GO:1902680	Positive regulation of RNA biosynthetic process	.0127	1642
GO:0044248	Cellular catabolic process	1.57×10^{-3}	2199	GO:0030030	Cell projection organization	.0135	1525
GO:0071276	Cellular response to cadmium ion	2.02×10^{-3}	36	GO:0048812	Neuron projection morphogenesis	.0136	623
GO:0051963	Regulation of synapse assembly	2.37×10^{-3}	103	GO:0045934	Negative regulation of nucleobase-containing compound metabolic process	.0169	1533
GO:0006521	Regulation of cellular amino acid metabolic process	3.26×10^{-3}	33	GO:0120039	Plasma membrane bounded cell projection morphogenesis	.022	638

3.8 | Association with PD postmortem-derived gene expression information

We found genes downweighted in PD relative to controls in cortex were more positively weighted than chance in our analysis: cortex, $p < .0001$; Brodmann area 6, $p = .0008$ after correcting for multiple comparisons. Similarly, genes downweighted in dementia with Lewy bodies relative to controls in cortex were more positively weighted than chance in our analysis ($p < .001$). These results suggest that gene expression profiles identified based on functional-metabolic architecture of PD and gene expression in healthy donors are more perturbed in PD than chance. And the findings remain robust at later disease stage related with dementia with Lewy bodies.

4 | DISCUSSION

In this study, we for the first time investigated the association between the functional-metabolic architecture in PD and the transcriptional genetic expression profiles that were collected in healthy volunteers. Regional alterations of functional gradients highly overlapped with the FDG-uptake in PD patients. The alteration of functional-metabolic architecture, defined as the first principal component (PC1) of the functional gradients and FDG-uptake, was highly associated with the expression profile of certain genes which are involved in biological processes such as synapse regulation, copper ion detoxification and stress response, cellular catabolic, metabolic and biosynthetic processes, RNA metabolic process, and DNA transcription regulation. And the functional-metabolic architecture of SMN was significantly correlated with the PD rating scale. These results advance the comprehension of the imaging-genetic linking of PD.

The functional gradient approach provides a simplified characterization of the principal dimensions to depict the alternation of the macroscale cortical organization. While the explained ratios of gradients did not differentiate between PD patients and healthy population, significantly increased variation was obtained in the visual, somatomotor, attention as well as SN, indicating excessive network

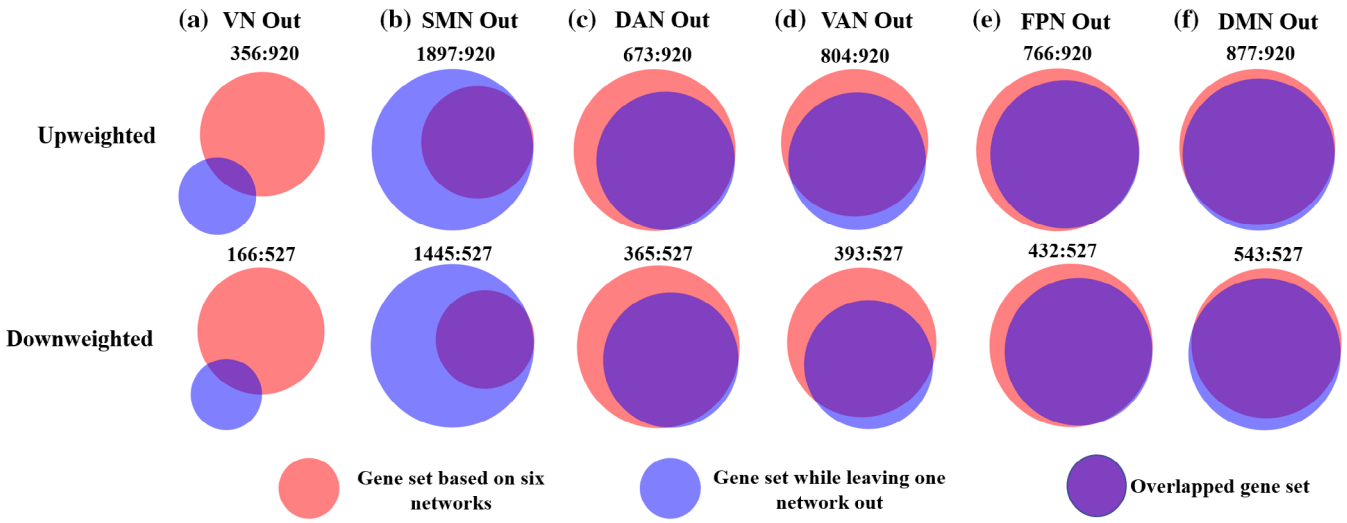

FIGURE 6 Venn diagram of gene sets based on six networks and five networks while leaving one network out every time. Overlap of the upweighted and downweighted genes identified by regression analysis based on six networks and leaving visual network (VN, panel a); somatomotor network (SMN, panel b); dorsal attention network (DAN, panel c); ventral attention network (VAN, panel d); frontoparietal network (FPN, panel e); and default mode network (DMN, panel f) out was shown separately. The number of genes in each regression analysis was labeled (leave-one-network-out: six networks, i.e., 920 for upweighted genes and 527 for downweighted genes).

dispersion of multifunctional principles in PD. Previous study that investigated the network gradients in PD patients have shown stronger structural-functional coupling in the anterior aspect (i.e., frontal lobe) of the anterior-to-posterior component, and weakened structural-functional coupling in the transmodal aspect (i.e., DMN) of the unimodal-to-transmodal component (Zarkali et al., 2021). Interestingly, the first two gradients ranked opposite to the gradients in the original description (Margulies et al., 2016). The exact reason of obtaining the opposite first and second gradients with previous findings was currently unclear. However, two possible factors may influence the outcomes. First, from the methodological point of view, the reliability of the gradient metrics was low as we demonstrated in our previous study (Zhang & Zang, 2023), indicating that large sample size may be necessary to obtain relatively robust outputs. As we stated in the limitation section, the hybrid PET/MR data are much more difficult to acquire, such that the sample size may constrain statistical efficacy and reliability on the functional gradient metrics. In addition, the opposite first and second gradients were very similar in terms of explanation ratios, indicating that increasing the sample size may possibly inverse the distribution. Second from the biological point of view, as demonstrated by previous studies (Dong et al., 2021), the gradient components distribution varied nonlinearly from childhood (Nenning et al., 2020) to adult and aged population. These life-span findings of gradient components suggest that age could influence significantly on the distribution of first and second components. Therefore, the obtained opposite first and second gradients may also be impacted by the age distribution of PD. Among the networks that showed disrupted network dispersions, the somatomotor network and the SN are associated with motor deficits (McGregor & Nelson, 2019). The visual functional impairment was a major non-motor aspect of PD as a majority of PD patients reported visual symptoms (Weil et al., 2016). Resting state fMRI analysis also provided imaging evidence of altered VN functional connectivity in PD patients (Göttlich et al., 2013). Previous examination of cognitively unimpaired PD patients showed impairment of DMN functional connectivity which further correlated significantly with the cognitive parameters, indicating the role of DMN functional impairment in cognitive decline (Tessitore et al., 2012). The increased network dispersion in PD obtained in the current study suggests an excessive heterogeneity of the brain connectivity patterns, which aligned well with the above-mentioned studies.

Meanwhile, the VN exhibited reduced FDG-uptake and the somatomotor as well as the VAN exhibited increased FDG-uptake in PD patients. These metabolic results were highly robust as reported in previous FDG-PET studies (Matthews et al., 2018; P. Wu et al., 2014). For glucose metabolic study that used quantitative FDG-PET, the absolute metabolic level revealed decreased glucose metabolism in the occipital regions but relatively preserved glucose metabolism in the motor regions (Bohnen et al., 2011; Hu et al., 2000), indicating that the decreased FDG-uptake in the VN may be a more pronounced metabolic marker. In the current study, the spatial pattern of the alterations in functional gradients and FDG-uptake were highly similar and a close connection between network functional gradients and metabolism was established. Although many neuroimaging studies identified high spatial similarity between functional and metabolic impairments in PD patients (Jia et al., 2021; Ruppert et al., 2020; P. Wu et al., 2013; T. Wu et al., 2011), only few studies have applied hybrid PET/MRI scan (Shang et al., 2021; Zang, Song, Li, Nie, et al., 2022). The current study simultaneously acquired FDG-PET and fMRI data, allowing straightforward combination of functional gradients and glucose metabolism for construction of functional-metabolic architecture.

The PLS analysis between functional-metabolic architecture and gene expression data revealed significant genetic components that explained almost half of the total variance (48.99%). The first component of the PLS1 regression analysis alone explained a third of the variance (32.38%) and was associated significantly with 920 upweighted genes and 527 downweighted genes. By further applying leave-one-network-out analyses, the visual and the somatomotor networks ranked at the top regarding the influence on the association between transcriptomic gene expression profile and functional-metabolic architecture. These results indicated that the visual and somatomotor networks show higher genetic susceptibility. Specifically, leaving the VN out showed most influential effect on the association between the functional-metabolic architecture and the gene expression profiles as most of the genes did not overlap with and without VN. Functional as well as metabolic studies have demonstrated alteration of the VN that may predict dementia in PD (Bohnen et al., 2011; Hou et al., 2021). These observations may indicate that the GO terms identified in the current study are cognitive relevance in PD patients. In addition, the functional-metabolic architecture of the SMN was associated significantly with the UPDRS III score, suggesting that therapeutic interventions that target the SMN may be more effective.

The biological processes that were significantly enriched in the 920 upweighted genes defined by PLS1 mainly included synapse regulation, copper ion detoxification and stress response, cellular catabolic process, cellular and molecular metabolic process, and sterol biosynthetic process. In PD patients, mutations of genes that are associated with synaptic homeostasis, autophagy and pruning may be critical factors of neurodegeneration via synaptic disturbances (Plowey & Chu, 2011; Soukup et al., 2018). While the functional-metabolic architecture reflects macroscale of integration of functional gradients transition of networks as well as the energy consumption, it was closely associated with neural synapse activity at microscale (Stampanoni Bassi et al., 2019; Zaldivar et al., 2022). The current study also identified pathways that are associated with copper ion detoxification and stress response, which was highly in line with a previous study (Thomas et al., 2021). Alteration of copper level could cause excessive oxidative load that associated with iron accumulation (Dexter et al., 1991; Montes et al., 2014; Thomas et al., 2021) and thereby impairs functional-metabolic architecture in PD patients. In addition, cellular metabolism such as oxidative stress and energy failure is considered as the critical hallmarks of neuronal cell death in neurodegenerative disorders (Cobb & Cole, 2015; Pathak et al., 2013). Mitochondrial metabolic dysfunction (Anandhan et al., 2017), more specifically energy metabolism, was associated with the abnormal glucose metabolism captured by FDG-PET (Eberling et al., 1994). While catabolic process is essential for breaking down molecules to release energy and participating in anabolic reactions, it is also affected to induce neurodegenerative disorders like PD (Terman, 2006). As an example, accumulation of alpha-synuclein in the dopaminergic neurons could form Lewy bodies (Bennett, 2005) which were considered as the hallmark of PD.

GO terms that mainly associate with RNA metabolic and biosynthetic processes and regulation of transcription of DNA and nucleic acid were identified in the downweighted genes. A previous study that investigated structural connectivity and visual hallucination in PD reported RNA-associated biological pathways in the downweighted genes (Zarkali et al., 2020). Reduction of DNA transcription and impairment of nucleolar integrity were often observed in neurodegenerative disorders including PD (Evsyukov et al., 2017; Parlato & Kreiner, 2013). Deficits in nucleotide excision repairing were closely related to PD patients (Sepe et al., 2016), and aging-related stress could further induce accumulation of isolated RNA, reflecting metabolism and oxidative stress (Sudmant et al., 2018). Therefore, the biological processes of RNA and DNA metabolism, activity, and repairment are influential factors of the neurodegeneration process in human PD.

By evaluation of the functional gradient and FDG-uptake between HCs and PD, VN-SMN networks showed the highest spatial coincidence of abnormal functional gradients and glucose metabolism. While the VN-SMN networks geometrically located at the most posterior and top-lateral site of the human cortex, they both represent the poles of unimodal areas. Meanwhile, the VN-SMN networks are also most influential on the gene expression profiles in association with PD. These observations suggested that dysregulation of certain gene expression companied with abnormal aging may preferentially affect the functions of unimodal areas and disrupt the corresponding energy consumption of neural interactions.

4.1 | Limitations

There are several limitations of the current study. First, the sample size of the current study was relatively small compared to other neuroimaging studies. However, considering the complicated and costly nature of hybrid PET/MRI data acquisition, the current study could still provide unique insights regarding simultaneous functional and metabolic architecture in PD. Second, the influence of medication was difficult to be fully washed out by the frequently used 12-h off-medication duration. De novo PD patients may be needed in the future to fully exclude the influence of medication. Third, similar to the previous transcriptomic neuroimaging studies, our analysis also used the transcriptome data derived from healthy donors. Therefore, conclusions only apply to the intrinsic variability, not to changes in gene expression occurring in PD. In addition, there is a gender bias in the gene expression dataset that male donors outnumbered female donors. The exact influence of gender bias on the imaging-genetic association is also difficult to be fully discarded. A larger sample of sex-balanced, whole-brain transcriptome data from PD patients is needed to further validate the association of functional-metabolic architecture and gene expression. Finally, our intention to combine functional gradient and glucose metabolism as a representation of functional-metabolic architecture was to integrate energy consumption information with functional network. However, it is still not fully known regarding the exact biological interpretation of the functional-

metabolic architecture due to the rarity of hybrid PET/MRI study in PD. Therefore, studies with large sample are needed to fully clarify the biological meaning of the functional-metabolic architecture.

5 | CONCLUSIONS

In conclusion, the current study is to our knowledge the first to establish the association between transcriptomic gene expression profile and functional-metabolic architecture in PD patients. We demonstrated that pathways of synaptic functioning, nerve development, cellular and RNA metabolic, catabolic process and DNA transcription regulation may be key factors contributing to the functional-metabolic architecture in PD, especially in the visual and somatomotor networks. The current study could bring novel insights into the genetic mechanism of macroscale functional as well as metabolic systems in PD and further provide neuroimaging reference for therapeutic interventions.

AUTHOR CONTRIBUTIONS

Zhenxiang Zang: Manuscript preparation, study concept and design, analysis and interpretation of data. Xiaolong Zhang: Manuscript preparation, study concept and design, analysis and interpretation of data. Tianbin Song: Manuscript revision, data acquisition. Jiping Li: Data acquisition, clinical assessment. Binbin Nie: Data analysis. Shanshan Mei: data acquisition, clinical assessment. Zhi'an Hu: Data sharing, manuscript review. Yuqing Zhang: Data acquisition, manuscript revision and critical review. Jie Lu: Funding, study concept, manuscript revision and critical review.

ACKNOWLEDGMENT

The authors would like to thank Mr. Jie Ma and Ms. Yu Yang for their help during data collection.

FUNDING INFORMATION

This study was supported by Huizhi Ascent Project of Xuanwu Hospital, Code: HZ2021ZCLJ005.

CONFLICT OF INTEREST STATEMENT

The authors declare no conflict of interests in the current study.

DATA AVAILABILITY STATEMENT

The data that support the findings of this study are available from the corresponding author upon reasonable request. A formal project protocol is recommended. Gene expression profiles were downloaded from the Allen Brain Atlas (http://www.brain-map.org), and the preprocessed genes expression matrix was obtained at https://github.com/gecthomas/QSM_and_AHBA_transcription_in_PD.

ORCID

Zhenxiang Zang https://orcid.org/0000-0002-6865-054X
Xiaolong Zhang https://orcid.org/0000-0002-0099-1129
Jie Lu https://orcid.org/0000-0003-0425-3921

REFERENCES

Albrecht, F., Ballarini, T., Neumann, J., & Schroeter, M. L. (2019). FDG-PET hypometabolism is more sensitive than MRI atrophy in Parkinson's disease: A whole-brain multimodal imaging meta-analysis. *NeuroImage: Clinical*, *21*, 101594. https://doi.org/10.1016/j.nicl.2018.11.004

Anandhan, A., Jacome, M. S., Lei, S., Hernandez-Franco, P., Pappa, A., Panayiotidis, M. I., Powers, R., & Franco, R. (2017). Metabolic dysfunction in Parkinson's disease: Bioenergetics, redox homeostasis and central carbon metabolism. *Brain Research Bulletin*, *133*, 12–30. https://doi.org/10.1016/j.brainresbull.2017.03.009

Bennett, M. C. (2005). The role of alpha-synuclein in neurodegenerative diseases. *Pharmacology & Therapeutics*, *105*(3), 311–331. https://doi.org/10.1016/j.pharmthera.2004.10.010

Bigdeli, T. B., Lee, D., Webb, B. T., Riley, B. P., Vladimirov, V. I., Fanous, A. H., Kendler, K. S., & Bacanu, S. A. (2016). A simple yet accurate correction for winner's curse can predict signals discovered in much larger genome scans. *Bioinformatics*, *32*(17), 2598–2603. https://doi.org/10.1093/bioinformatics/btw303

Bohnen, N. I., Koeppe, R. A., Minoshima, S., Giordani, B., Albin, R. L., Frey, K. A., & Kuhl, D. E. (2011). Cerebral glucose metabolic features of Parkinson disease and incident dementia: Longitudinal study. *Journal of Nuclear Medicine*, *52*(6), 848–855. https://doi.org/10.2967/jnumed.111.089946

Caciagli, L., Paquola, C., He, X., Vollmar, C., Centeno, M., Wandschneider, B., Braun, U., Trimmel, K., Vos, S. B., Sidhu, M. K., Thompson, P. J., Baxendale, S., Winston, G. P., Duncan, J. S., D. S., Koepp, M. J., & Bernhardt, B. C. (2022). Disorganization of language and working memory systems in frontal versus temporal lobe epilepsy. *Brain*, *146*, 935–953. https://doi.org/10.1093/brain/awac150

Cascone, A. D., Langella, S., Sklerov, M., & Dayan, E. (2021). Frontoparietal network resilience is associated with protection against cognitive decline in Parkinson's disease. *Communications Biology*, *4*(1), 1021. https://doi.org/10.1038/s42003-021-02478-3

Cobb, C. A., & Cole, M. P. (2015). Oxidative and nitrative stress in neurodegeneration. *Neurobiology of Disease*, *84*, 4–21. https://doi.org/10.1016/j.nbd.2015.04.020

Coifman, R. R., Lafon, S., Lee, A. B., Maggioni, M., Nadler, B., Warner, F., & Zucker, S. W. (2005). Geometric diffusions as a tool for harmonic analysis and structure definition of data: Diffusion maps. *Proceedings of the National Academy of Sciences of the United States of America*, *102*(21), 7426–7431. https://doi.org/10.1073/pnas.0500334102

Damoiseaux, J. S., Rombouts, S. A., Barkhof, F., Scheltens, P., Stam, C. J., Smith, S. M., & Beckmann, C. F. (2006). Consistent resting-state networks across healthy subjects. *Proceedings of the National Academy of Sciences of the United States of America*, *103*(37), 13848–13853. https://doi.org/10.1073/pnas.0601417103

DeLong, M. R. (1990). Primate models of movement disorders of basal ganglia origin. *Trends in Neurosciences*, *13*(7), 281–285. https://doi.org/10.1016/0166-2236(90)90110-V

Dexter, D. T., Carayon, A., Javoy-Agid, F., Agid, Y., Wells, F. R., Daniel, S. E., Lees, A. J., Jenner, P., & Marsden, C. D. (1991). Alterations in the levels of iron, ferritin and other trace metals in Parkinson's disease and other neurodegenerative diseases affecting the basal ganglia. *Brain*, *114*(Pt 4), 1953–1975. https://doi.org/10.1093/brain/114.4.1953

Dong, H. M., Margulies, D. S., Zuo, X. N., & Holmes, A. J. (2021). Shifting gradients of macroscale cortical organization mark the transition from childhood to adolescence. *Proceedings of the National Academy of Sciences of the United States of America*, *118*(28), e2024448118. https://doi.org/10.1073/pnas.2024448118

Eberling, J. L., Richardson, B. C., Reed, B. R., Wolfe, N., & Jagust, W. J. (1994). Cortical glucose metabolism in Parkinson's disease without dementia. *Neurobiology of Aging*, *15*(3), 329–335. https://doi.org/10.1016/0197-4580(94)90028-0

Evsyukov, V., Domanskyi, A., Bierhoff, H., Gispert, S., Mustafa, R., Schlaudraff, F., Liss, B., & Parlato, R. (2017). Genetic mutations linked to Parkinson's disease differentially control nucleolar activity in pre-symptomatic mouse models. *Disease Models & Mechanisms*, *10*(5), 633–643. https://doi.org/10.1242/dmm.028092

Freeze, B., Pandya, S., Zeighami, Y., & Raj, A. (2019). Regional transcriptional architecture of Parkinson's disease pathogenesis and network spread. *Brain*, *142*(10), 3072–3085. https://doi.org/10.1093/brain/awz223

Glasser, M. F., Coalson, T. S., Robinson, E. C., Hacker, C. D., Harwell, J., Yacoub, E., Ugurbil, K., Andersson, J., Beckmann, C. F., Jenkinson, M., Smith, S. M., & Van Essen, D. C. (2016). A multi-modal parcellation of human cerebral cortex. *Nature*, *536*(7615), 171–178. https://doi.org/10.1038/nature18933

Göttlich, M., Münte, T. F., Heldmann, M., Kasten, M., Hagenah, J., & Krämer, U. M. (2013). Altered resting state brain networks in Parkinson's disease. *PLoS One*, *8*(10), e77336. https://doi.org/10.1371/journal.pone.0077336

Hawrylycz, M., Miller, J. A., Menon, V., Feng, D., Dolbeare, T., Guillozet-Bongaarts, A. L., Jegga, A. G., Aronow, B, J., Lee, C-K., Bernard, A., Glasser, M., Dierker, D. L., Menche, J., Szafer, A., Collman, F., Grange, P., Berman, K. A., Mihalas, S., & Lein, E. (2015). Canonical genetic signatures of the adult human brain. *Nature Neuroscience*, *18*(12), 1832–1844. https://doi.org/10.1038/nn.4171

Hong, S.-J., Vos de Wael, R., Bethlehem, R. A. I., Lariviere, S., Paquola, C., Valk, S. L., Milham, M. P., Di Martino, A., Margulies, D. S., Smallwood, J., & Bernhardt, B. C. (2019). Atypical functional connectome hierarchy in autism. *Nature Communications*, *10*(1), 1022. https://doi.org/10.1038/s41467-019-08944-1

Hou, Y., Wei, Q., Ou, R., Zhang, L., Yuan, X., Gong, Q., & Shang, H. (2021). Different resting-state network disruptions in newly diagnosed drug-naïve Parkinson's disease patients with mild cognitive impairment. *BMC Neurology*, *21*(1), 327. https://doi.org/10.1186/s12883-021-02360-z

Hu, M. T., Taylor-Robinson, S. D., Chaudhuri, K. R., Bell, J. D., Labbé, C., Cunningham, V. J., Koepp, M. J., Hammers, A., Morris, R. G., Turjanski, N., & Brooks, D. J. (2000). Cortical dysfunction in non-demented Parkinson's disease patients: A combined (31)P-MRS and (18)FDG-PET study. *Brain*, *123*(Pt 2), 340–352. https://doi.org/10.1093/brain/123.2.340

Hulsen, T., de Vlieg, J., & Alkema, W. (2008). BioVenn—A web application for the comparison and visualization of biological lists using area-proportional Venn diagrams. *BMC Genomics*, *9*, 488. https://doi.org/10.1186/1471-2164-9-488

Hyder, F., Rothman, D. L., & Bennett, M. R. (2013). Cortical energy demands of signaling and nonsignaling components in brain are conserved across mammalian species and activity levels. *Proceedings of the National Academy of Sciences of the United States of America*, *110*(9), 3549–3554. https://doi.org/10.1073/pnas.1214912110

Ji, G. J., Hu, P., Liu, T. T., Li, Y., Chen, X., Zhu, C., Tian, Y., Chen, X., & Wang, K. (2018). Functional connectivity of the corticobasal ganglia-thalamocortical network in Parkinson disease: A systematic review and meta-analysis with cross-validation. *Radiology*, *287*(3), 973–982. https://doi.org/10.1148/radiol.2018172183

Jia, X.-Z., Zhao, N., Dong, H.-M., Sun, J.-W., Barton, M., Burciu, R., Carrière, N., Cerasa, A., Chen, B.-Y., Chen, J., Coombes, S., Defebvre, L., Delmaire, C., Dujardin, K., Esposito, F., Fan, G.-G., Di Nardo, F., Feng, Y.-X., & Zang, Y.-F. (2021). Small P values may not yield robust findings: An example using REST-meta-PD. *Science Bulletin*, *66*(21), 2148–2152. https://doi.org/10.1016/j.scib.2021.06.007

Klein, C., & Westenberger, A. (2012). Genetics of Parkinson's disease. *Cold Spring Harbor Perspectives in Medicine*, *2*(1), a008888. https://doi.org/10.1101/cshperspect.a008888

Ko, J. H., Spetsieris, P. G., & Eidelberg, D. (2018). Network structure and function in Parkinson's disease. *Cerebral Cortex*, *28*(12), 4121–4135. https://doi.org/10.1093/cercor/bhx267

Ma, Y., Tang, C., Spetsieris, P. G., Dhawan, V., & Eidelberg, D. (2007). Abnormal metabolic network activity in Parkinson's disease: Test-retest reproducibility. *Journal of Cerebral Blood Flow and Metabolism*, *27*(3), 597–605. https://doi.org/10.1038/sj.jcbfm.9600358

Margulies, D. S., Ghosh, S. S., Goulas, A., Falkiewicz, M., Huntenburg, J. M., Langs, G., Bezgin, G., Eickhoff, S. B., Castellanos, X. F., Petrides, M., Jefferies, E., & Smallwood, J. (2016). Situating the default-mode network along a principal gradient of macroscale cortical organization. *Proceedings of the National Academy of Sciences of the United States of America*, *113*(44), 12574–12579. https://doi.org/10.1073/pnas.1608282113

Matthews, D. C., Lerman, H., Lukic, A., Andrews, R. D., Mirelman, A., Wernick, M. N., Giladi, N., Strother, S. C., Evans, K. C., Cedarbaum, J. M., & Even-Sapir, E. (2018). FDG PET Parkinson's disease-related pattern as a biomarker for clinical trials in early stage disease. *NeuroImage: Clinical*, *20*, 572–579. https://doi.org/10.1016/j.nicl.2018.08.006

McGregor, M. M., & Nelson, A. B. (2019). Circuit mechanisms of Parkinson's disease. *Neuron*, *101*(6), 1042–1056. https://doi.org/10.1016/j.neuron.2019.03.004

Montes, S., Rivera-Mancia, S., Diaz-Ruiz, A., Tristan-Lopez, L., & Rios, C. (2014). Copper and copper proteins in Parkinson's disease. *Oxidative Medicine and Cellular Longevity*, *2014*, 147251. https://doi.org/10.1155/2014/147251

Nalls, M. A., Blauwendraat, C., Vallerga, C. L., Heilbron, K., Bandres-Ciga, S., Chang, D., Tan, M., Kia, D. A., Noyce, A. J., Xue, A., Bras, J., Young, E., von Coelln, R., Simón-Sánchez, J., Schulte, C., Sharma, M., Krohn, L., Pihlstrøm, L., & Singleton, A. B. (2019). Identification of novel risk loci, causal insights, and heritable risk for Parkinson's disease: A meta-analysis of genome-wide association studies. *Lancet Neurology*, *18*(12), 1091–1102. https://doi.org/10.1016/s1474-4422(19)30320-5

Nenning, K. H., Xu, T., Schwartz, E., Arroyo, J., Woehrer, A., Franco, A. R., Vogelstein, J. T., Margulies, D. S., Liu, H., Smallwood, J., Milham, M. P., & Langs, G. (2020). Joint embedding: A scalable alignment to compare individuals in a connectivity space. *NeuroImage*, *222*, 117232. https://doi.org/10.1016/j.neuroimage.2020.117232

Nie, B., Liang, S., Jiang, X., Duan, S., Huang, Q., Zhang, T., Li, P., & Shan, B. (2018). An automatic method for generating an unbiased intensity normalizing factor in positron emission tomography image analysis after stroke. *Neuroscience Bulletin*, *34*(5), 833–841. https://doi.org/10.1007/s12264-018-0240-8

Parlato, R., & Kreiner, G. (2013). Nucleolar activity in neurodegenerative diseases: A missing piece of the puzzle? *Journal of Molecular Medicine (Berlin, Germany)*, *91*(5), 541–547. https://doi.org/10.1007/s00109-012-0981-1

Pathak, D., Berthet, A., & Nakamura, K. (2013). Energy failure: Does it contribute to neurodegeneration? *Annals of Neurology*, *74*(4), 506–516. https://doi.org/10.1002/ana.24014

Plowey, E. D., & Chu, C. T. (2011). Synaptic dysfunction in genetic models of Parkinson's disease: A role for autophagy? *Neurobiology of Disease*, *43*(1), 60–67. https://doi.org/10.1016/j.nbd.2010.10.011

Postuma, R. B., Berg, D., Stern, M., Poewe, W., Olanow, C. W., Oertel, W., Obeso, J., Marek, K., Litvan, I., Lang, A. E., Halliday, G., Goetz, C. G., Gasser, T., Dubois, B., Piu Chan, P., Bloem, B. R., Adler, C. H., & Deuschl, G. (2015). MDS clinical diagnostic criteria for Parkinson's disease. *Movement Disorders*, *30*(12), 1591–1601. https://doi.org/10.1002/mds.26424

Postuma, R. B., Poewe, W., Litvan, I., Lewis, S., Lang, A. E., Halliday, G., Goetz, C. G., Chan, P., Slow, E., Seppi, K., Schaffer, E., Rios-Romenets, S., Mi, T., Maetzler, C., Li, Y., Heim, B., Bledsoe, I. O., & Berg, D. (2018). Validation of the MDS clinical diagnostic criteria for Parkinson's

disease. *Movement Disorders*, *33*(10), 1601–1608. https://doi.org/10.1002/mds.27362

Power, J. D., Barnes, K. A., Snyder, A. Z., Schlaggar, B. L., & Petersen, S. E. (2012). Spurious but systematic correlations in functional connectivity MRI networks arise from subject motion. *NeuroImage*, *59*(3), 2142–2154. https://doi.org/10.1016/j.neuroimage.2011.10.018

Power, J. D., Cohen, A. L., Nelson, S. M., Wig, G. S., Barnes, K. A., Church, J. A., Vogel, A. C., Laumann, T. O., Miezin, F. M., Schlaggar, B. L., & Petersen, S. E. (2011). Functional network organization of the human brain. *Neuron*, *72*(4), 665–678. https://doi.org/10.1016/j.neuron.2011.09.006

Power, J. D., Mitra, A., Laumann, T. O., Snyder, A. Z., Schlaggar, B. L., & Petersen, S. E. (2014). Methods to detect, characterize, and remove motion artifact in resting state fMRI. *NeuroImage*, *84*, 320–341. https://doi.org/10.1016/j.neuroimage.2013.08.048

Raudvere, U., Kolberg, L., Kuzmin, I., Arak, T., Adler, P., Peterson, H., & Vilo, J. (2019). g:Profiler: A web server for functional enrichment analysis and conversions of gene lists (2019 update). *Nucleic Acids Research*, *47*(W1), W191–W198. https://doi.org/10.1093/nar/gkz369

Ruppert, M. C., Greuel, A., Freigang, J., Tahmasian, M., Maier, F., Hammes, J., van Eimeren, T., Timmermann, L., Tittgemeyer, M., Alexander Drzezga, A., & Eggers, C. (2021). The default mode network and cognition in Parkinson's disease: A multimodal resting-state network approach. *Human Brain Mapping*, *42*(8), 2623–2641. https://doi.org/10.1002/hbm.25393

Ruppert, M. C., Greuel, A., Tahmasian, M., Schwartz, F., Stürmer, S., Maier, F., Hammes, J., Tittgemeyer, M., Timmermann, L., van Eimeren, T., Drzezga, A., & Eggers, C. (2020). Network degeneration in Parkinson's disease: Multimodal imaging of nigro-striato-cortical dysfunction. *Brain*, *143*(3), 944–959. https://doi.org/10.1093/brain/awaa019

Scherzer, C. R., Eklund, A. C., Morse, L. J., Liao, Z., Locascio, J. J., Fefer, D., Schwarzschild, M. A., Schlossmacher, M. G., Hauser, M. A., Vance, J. M., Sudarsky, L. R., Standaert, D. G., Growdon, J. H., Jensen, R. V., & Gullans, S. R. (2007). Molecular markers of early Parkinson's disease based on gene expression in blood. *Proceedings of the National Academy of Sciences of the United States of America*, *104*(3), 955–960. https://doi.org/10.1073/pnas.0610204104

Schindlbeck, K. A., & Eidelberg, D. (2018). Network imaging biomarkers: Insights and clinical applications in Parkinson's disease. *Lancet Neurology*, *17*(7), 629–640. https://doi.org/10.1016/s1474-4422(18)30169-8

Sepe, S., Milanese, C., Gabriels, S., Derks, K. W., Payan-Gomez, C., van IJcken, W. F. J., Rijksen, Y. M. A., Nigg, A. L., Moreno, S., Cerri, S., Blandini, F., Hoeijmakers, J. H. J., & Mastroberardino, P. G. (2016). Inefficient DNA repair is an aging-related modifier of Parkinson's disease. *Cell Reports*, *15*(9), 1866–1875. https://doi.org/10.1016/j.celrep.2016.04.071

Shang, S., Li, D., Tian, Y., Li, R., Zhao, H., Zheng, L., Zhang, Y., Chen, Y.-C., & Yin, X. (2021). Hybrid PET-MRI for early detection of dopaminergic dysfunction and microstructural degradation involved in Parkinson's disease. *Communications Biology*, *4*(1), 1162. https://doi.org/10.1038/s42003-021-02705-x

Simunovic, F., Yi, M., Wang, Y., Macey, L., Brown, L. T., Krichevsky, A. M., Andersen, S. L., Stephens, R. M., Benes, F. M., & Sonntag, K. C. (2008). Gene expression profiling of substantia nigra dopamine neurons: Further insights into Parkinson's disease pathology. *Brain*, *132*(7), 1795–1809. https://doi.org/10.1093/brain/awn323

Soukup, S. F., Vanhauwaert, R., & Verstreken, P. (2018). Parkinson's disease: Convergence on synaptic homeostasis. *The EMBO Journal*, *37*(18), e98960. https://doi.org/10.15252/embj.201898960

Stampanoni Bassi, M., Iezzi, E., Gilio, L., Centonze, D., & Buttari, F. (2019). Synaptic plasticity shapes brain connectivity: Implications for network topology. *International Journal of Molecular Sciences*, *20*(24), 6193. https://doi.org/10.3390/ijms20246193

Sudmant, P. H., Lee, H., Dominguez, D., Heiman, M., & Burge, C. B. (2018). Widespread accumulation of ribosome-associated isolated 3′ UTRs in neuronal cell populations of the aging brain. *Cell Reports*, *25*(9), 2447–2456.e2444. https://doi.org/10.1016/j.celrep.2018.10.094

Supek, F., Bošnjak, M., Škunca, N., & Šmuc, T. (2011). REVIGO summarizes and visualizes long lists of gene ontology terms. *PLoS One*, *6*(7), e21800. https://doi.org/10.1371/journal.pone.0021800

Terman, A. (2006). Catabolic insufficiency and aging. *Annals of the new York Academy of Sciences*, *1067*, 27–36. https://doi.org/10.1196/annals.1354.005

Tessitore, A., Esposito, F., Vitale, C., Santangelo, G., Amboni, M., Russo, A., Corbo, D., Cirillo, G., Barone, P., & Tedeschi, G. (2012). Default-mode network connectivity in cognitively unimpaired patients with Parkinson disease. *Neurology*, *79*(23), 2226–2232. https://doi.org/10.1212/WNL.0b013e31827689d6

Thomas, G. E. C., Zarkali, A., Ryten, M., Shmueli, K., Gil-Martinez, A. L., Leyland, L. A., McColgan, P., Acosta-Cabronero, J., Lees, A. J., & Weil, R. S. (2021). Regional brain iron and gene expression provide insights into neurodegeneration in Parkinson's disease. *Brain*, *144*(6), 1787–1798. https://doi.org/10.1093/brain/awab084

Tzourio-Mazoyer, N., Landeau, B., Papathanassiou, D., Crivello, F., Etard, O., Delcroix, N., Mazoyer, B., & Joliot, M. (2002). Automated anatomical labeling of activations in SPM using a macroscopic anatomical parcellation of the MNI MRI single-subject brain. *NeuroImage*, *15*(1), 273–289. https://doi.org/10.1006/nimg.2001.0978

Váša, F., Seidlitz, J., Romero-Garcia, R., Whitaker, K. J., Rosenthal, G., Vértes, P. E., Shinn, M., Alexander-Bloch, A., Fonagy, P., Dolan, R. J., Jones, P. B., Goodyer, I. M., NSPN consortium., Sporns, O., & Bullmore, E. T. (2018). Adolescent tuning of association cortex in human structural brain networks. *Cerebral Cortex*, *28*(1), 281–294. https://doi.org/10.1093/cercor/bhx249

Vervoort, G., Alaerts, K., Bengevoord, A., Nackaerts, E., Heremans, E., Vandenberghe, W., & Nieuwboer, A. (2016). Functional connectivity alterations in the motor and fronto-parietal network relate to behavioral heterogeneity in Parkinson's disease. *Parkinsonism & Related Disorders*, *24*, 48–55. https://doi.org/10.1016/j.parkreldis.2016.01.016

Vos de Wael, R., Benkarim, O., Paquola, C., Lariviere, S., Royer, J., Tavakol, S., Xu, T., Hong, S-J., Langs, G., Valk, S., Misic, B., Milham, M., Margulies, D., Smallwood, J., & Bernhardt, B. C. (2020). BrainSpace: A toolbox for the analysis of macroscale gradients in neuroimaging and connectomics datasets. *Communications Biology*, *3*(1), 103. https://doi.org/10.1038/s42003-020-0794-7

Weil, R. S., Schrag, A. E., Warren, J. D., Crutch, S. J., Lees, A. J., & Morris, H. R. (2016). Visual dysfunction in Parkinson's disease. *Brain*, *139*(11), 2827–2843. https://doi.org/10.1093/brain/aww175

Wu, P., Wang, J., Peng, S., Ma, Y., Zhang, H., Guan, Y., & Zuo, C. (2013). Metabolic brain network in the Chinese patients with Parkinson's disease based on 18F-FDG PET imaging. *Parkinsonism & Related Disorders*, *19*(6), 622–627. https://doi.org/10.1016/j.parkreldis.2013.02.013

Wu, P., Yu, H., Peng, S., Dauvilliers, Y., Wang, J., Ge, J., Zhang, H., Eidelberg, D., Ma, Y., & Zuo, C. (2014). Consistent abnormalities in metabolic network activity in idiopathic rapid eye movement sleep behaviour disorder. *Brain*, *137*(Pt 12), 3122–3128. https://doi.org/10.1093/brain/awu290

Wu, T., Long, X., Wang, L., Hallett, M., Zang, Y., Li, K., & Chan, P. (2011). Functional connectivity of cortical motor areas in the resting state in Parkinson's disease. *Human Brain Mapping*, *32*(9), 1443–1457. https://doi.org/10.1002/hbm.21118

Xia, M., Liu, J., Mechelli, A., Sun, X., Ma, Q., Wang, X., Wei, D., Chen, Y., Liu, B., Huang, C-C., Zheng, Y., Wu, Y., Chen, T., Cheng, Y., Xu, X., Gong, Q., Si, T., & He, Y. (2022). Connectome gradient dysfunction in major depression and its association with gene expression profiles and treatment outcomes. *Molecular Psychiatry*, *27*(3), 1384–1393. https://doi.org/10.1038/s41380-022-01519-5

Xia, M., Wang, J., & He, Y. (2013). BrainNet viewer: A network visualization tool for human brain connectomics. *PLoS One*, *8*(7), e68910. https://doi.org/10.1371/journal.pone.0068910

Xia, Y., Xia, M., Liu, J., Liao, X., Lei, T., Liang, X., Zhao, L., Shi, Z., Sun, L., Chen, X., Men, W., Wang, Y., Pan Z., Luo, J., Peng, S., Chen, M., Hao, L., Tan, S., & He, Y. (2022). Development of functional connectome gradients during childhood and adolescence. *Science Bulletin*, *67*(10), 1049–1061. https://doi.org/10.1016/j.scib.2022.01.002

Yan, C. G., Cheung, B., Kelly, C., Colcombe, S., Craddock, R. C., Di Martino, A., Roffman, J. L., Smoller, J. W., Zöllei, L., Polimeni, J. R., Fischl, B., Liu, H., & Milham, M. P. (2013). A comprehensive assessment of regional variation in the impact of head micromovements on functional connectomics. *NeuroImage*, *76*, 183–201. https://doi.org/10.1016/j.neuroimage.2013.03.004

Yeo, B. T., Krienen, F. M., Sepulcre, J., Sabuncu, M. R., Lashkari, D., Hollinshead, M., Joshua, L. R., Jordan, W. S., Lilla, Z., Jonathan, R. P., Bruce, F., Hesheng, L., & Buckner, R. L. (2011). The organization of the human cerebral cortex estimated by intrinsic functional connectivity. *Journal of Neurophysiology*, *106*(3), 1125–1165. https://doi.org/10.1152/jn.00338.2011

Zaldivar, D., Koyano, K. W., Ye, F. Q., Godlove, D. C., Park, S. H., Russ, B. E., Bhik-Ghanie, R., & Leopold, D. A. (2022). Brain-wide functional connectivity of face patch neurons during rest. *Proceedings of the National Academy of Sciences of the United States of America*, *119*(36), e2206559119. https://doi.org/10.1073/pnas.2206559119

Zalesky, A., Fornito, A., Harding, I. H., Cocchi, L., Yücel, M., Pantelis, C., & Bullmore, E. T. (2010). Whole-brain anatomical networks: Does the choice of nodes matter? *NeuroImage*, *50*(3), 970–983. https://doi.org/10.1016/j.neuroimage.2009.12.027

Zang, Z., Geiger, L. S., Braun, U., Cao, H., Zangl, M., Schäfer, A., Moessnang, C., Ruf, M., Reis, J., Schweiger, J. I., Dixson, L., Moscicki, A., Schwarz, E., Meyer-Lindenberg, A., & Tost, H. (2018). Resting-state brain network features associated with short-term skill learning ability in humans and the influence of N-methyl-d-aspartate receptor antagonism. *Network Neuroscience*, *2*(4), 464–480. https://doi.org/10.1162/netn_a_00045

Zang, Z., Song, T., Li, J., Nie, B., Mei, S., Zhang, C., Wu, T., Zhang, Y., & Lu, J. (2022). Simultaneous PET/fMRI revealed increased motor area input to subthalamic nucleus in Parkinson's disease. *Cerebral Cortex*, *33*, 167–175. https://doi.org/10.1093/cercor/bhac059

Zang, Z., Song, T., Li, J., Yan, S., Nie, B., Mei, S., Ma, J., Yang, Y., Shan, B., Zhang, Y., & Lu, J. (2022). Modulation effect of substantia nigra iron deposition and functional connectivity on putamen glucose metabolism in Parkinson's disease. *Human Brain Mapping*, *43*, 3735–3744. https://doi.org/10.1002/hbm.25880

Zarkali, A., McColgan, P., Leyland, L. A., Lees, A. J., Rees, G., & Weil, R. S. (2021). Organisational and neuromodulatory underpinnings of structural-functional connectivity decoupling in patients with Parkinson's disease. *Communications Biology*, *4*(1), 86. https://doi.org/10.1038/s42003-020-01622-9

Zarkali, A., McColgan, P., Ryten, M., Reynolds, R., Leyland, L. A., Lees, A. J., Rees, G., & Weil, R. S. (2020). Differences in network controllability and regional gene expression underlie hallucinations in Parkinson's disease. *Brain*, *143*(11), 3435–3448. https://doi.org/10.1093/brain/awaa270

Zhang, X., & Zang, Z. (2023). Evaluate the efficacy and reliability of functional gradients in within-subject designs. *Human Brain Mapping*, *44*(6), 2336–2344. https://doi.org/10.1002/hbm.26213

SUPPORTING INFORMATION

Additional supporting information can be found online in the Supporting Information section at the end of this article.

How to cite this article: Zang, Z., Zhang, X., Song, T., Li, J., Nie, B., Mei, S., Hu, Z., Zhang, Y., & Lu, J. (2023). Association between gene expression and functional-metabolic architecture in Parkinson's disease. *Human Brain Mapping*, *44*(16), 5387–5401. https://doi.org/10.1002/hbm.26443